2022-02-03

Effect of lattice mismatch on film morphology of the quasi-one dimensional conductor K0.3MoO3

RSC Advances

PAPER

Cite this: *RSC Adv.*, 2022, **12**, 4521

Effect of lattice mismatch on film morphology of the quasi-one dimensional conductor $K_{0.3}MoO_3$

Yifeng Cao,[a] Nicholas Russo,[a] Lei Gao,[b] Ailing Ji,[b] Linda H. Doerrer,[a] Nianpeng Lu[b] and Kevin E. Smith*[a]

Received 23rd October 2021
Accepted 25th January 2022

DOI: 10.1039/d1ra07842a

rsc.li/rsc-advances

High quality epitaxial thin films of the quasi-one dimensional conductor $K_{0.3}MoO_3$ have been successfully grown on $SrTiO_3$(100), $SrTiO_3$(110), and $SrTiO_3$(510) substrates *via* pulsed laser deposition. Scanning electron microscopy revealed quasi-one dimensional rod-shaped structures parallel to the substrate surface, and the crystal structure was verified by using X-ray diffraction. The temperature dependence of the resistivity for the $K_{0.3}MoO_3$ thin films demonstrates a metal-to-semiconductor transition at about 180 K. Highly anisotropic resistivity was also observed for films grown on $SrTiO_3$(510).

1 Introduction

Quasi-low-dimensional solids are important materials for both fundamental research and applied science.[1,2] For example, quasi-one-dimensional organic salts TTF-TCNQ, $(TMTTF)_2X$, *etc.* are bulk three-dimensional compounds.[3] The carrier motion therein is restricted to two-dimensional atomic layers, or one-dimensional chains, yet the Coulomb force remains three-dimensional in character, due to the anisotropy of transfer integrals between different chemical units. This enables these quasi-low-dimensional solids to be ideal platforms for the observation of Wigner crystallization.

Among quasi-low-dimensional solids, blue molybdenum bronze ($A_{0.3}MoO_3$, A = K, Rb, Tl) attracted our attention with the availability of large-sized, high-quality crystals.[4] Blue molybdenum bronzes (BMBs) are known for charge density wave (CDW) behaviors in which Peierls predicted that the electron density would show periodic fluctuations by the rearrangement of the ion cores causes a metal to semiconductor Peierls transition with transition temperature about 182 K.[5] BMBs have monoclinic symmetry with 20 molecular formula per unit cell in space group $C2/m$.[6] The structure of the BMBs is composed of infinite chains of MoO_6 octahedra with A cations located at sharing corners along the monoclinic b direction. The conductive chain structure not only makes the BMBs good candidates as CDW materials where the motion of electrons is restricted to the c axis but also, unlike $NbSe_3$ (ref. 7) and TaS_3,[8] remain unchanged when we modify the interchain interactions. It is of importance to prepare thin films of quasi-low dimensional BMBs in order to probe the role of film thickness on CDW behavior. In this paper, we focus on preparing crystalline thin films for blue bronze $K_{0.3}MoO_3$ (a = 18.249 Å, b = 7.560 Å, c = 9.855 Å, $\beta = 117°32'$ (ref. 6)).

Bulk $K_{0.3}MoO_3$ was first synthesized by Wold *et al.* in 1964 by electrolytic reduction of K_2MoO_4–MoO_3 melts under desired temperature.[9] Synthesis of nanoscaled crystalline $K_{0.3}MoO_3$, however, remained a hard task. CDW material like $NbSe_3$ (ref. 10) and TaS_3 (ref. 11) were prepared by chemical vapor transport method. Takamasa *et al.* applied this method on BMBs but did not work. Then they tried hydrothermal method on $K_{0.3}MoO_3$ and successfully prepared the nanoribbons of $K_{0.3}MoO_3$.[12] The crystalline $Rb_{0.3}MoO_3$ thin film was prepared by van der Zant *et al.* using pulsed laser deposition.[13] Dominko *et al.* applied the same method on $K_{0.3}MoO_3$ and got the thin films of about 100 nm in thickness on $Al_2O_3(1\bar{1}02)$ substrate and $SrTiO_3$(510) substrate.[14] However, the resistivity of their thin film is even an order higher than the least conducting direction of bulk $K_{0.3}MoO_3$ and no metal to semiconductor transition is observed.

In this study, we applied pulsed laser deposition to synthesize $K_{0.3}MoO_3$ on $SrTiO_3$(100), $SrTiO_3$(110) and $SrTiO_3$(510) substrates, respectively. High-quality crystalline samples about 100 nm in thickness were obtained, and typical temperature dependence of electrical resistivity indicates the occurrence of metal to semiconductor transition at about 180 K. The anisotropic electrical resistivity confirms the quasi-one dimensional nature of the films.

2 Experimental

2.1 Sample preparation

The $K_{0.3}MoO_3$ target for PLD growth was fabricated in a vacuum furnace, with a mixture of K_2O and MoO_3 in the molar ratio of 0.15 : 1, calcined at 1500 °C and then pressed into a pellet. The PLD laser source was a KrF Compex Pro 205F manufactured by Coherent, operating at a wavelength of 248 nm. The substrates

[a]*Department of Physics, Boston University, Boston, Massachusetts 02215, USA. E-mail: ksmith@bu.edu; Tel: +1-617-353-6117*

[b]*Institute of Physics, Chinese Academy of Sciences, Beijing, 100190, China*

were 5 × 5 × 0.5 mm and preprocessed with a plasma cleaner. The distance between the substrate and the target was set at 65 mm. We found the best quality $K_{0.3}MoO_3$ thin films were grown with a 52 mJ pulse energy, corresponding to an energy density of 13 mJ mm^{-2}, and an oxygen pressure of 8 Pa. The temperature of the substrate was set to 450 °C for $SrTiO_3$(100) substrates and 400 °C for the $SrTiO_3$(110) and $SrTiO_3$(510) substrates. The frequency of the laser seeming did not affect the quality of the thin film because the duration of the laser pulse is only 25 ns which means the plume has enough relaxation time from pulse to pulse. In this study, we set the laser frequency to 4 Hz in order to achieve a moderate growing speed of about 5 nm min^{-1}.

2.2 Characterization

X-ray diffraction (XRD) characterization of the $K_{0.3}MoO_3$ thin films was performed on a Rigaku Smartlab with Cu-Kα radiation (45 kV, 200 mA) with a step size of 0.02° and a scan rate of 6° min^{-1}. Scanning electron microscopy (SEM) were recorded using a HITACHI SU8220 (3–10 kV, 10 μA) with EDS system from EDAX (15 kV, 10 μA) to analyze the elemental composition of the samples. Atomic force microscopy (AFM) was used to investigate the surface morphology using an Oxford Instruments MPF-3D Origin. The linear scanning rate is set to 1 Hz with scan resolution of 256 sampling points per line. Electrical resistance was measured using a four-probe method with indium pads attached to the four corners of the substrate. The electrical current and voltage relationship obtained by a Keithley 2602B SourceMeter with Lab Tracer software. The probe current was set to 10^{-4} A and the voltage measured to get the resistance. The SourceMeter is connected with Linkam temperature control stage with liquid nitrogen as cooling source. With this stage, the temperature dependence of the electrical resistance can be measured in a range from 350 K to 90 K.

3 Results and discussion

3.1 Composition and film morphology

Energy dispersive spectroscopy (EDS) analysis shows that the K : Mo ratio in the films is 0.3 : 1 within an accuracy of 5%, therefore the stoichiometry of our samples for further investigation below can be taken as $K_{0.3}MoO_3$.

Fig. 1 presents the XRD patterns for $K_{0.3}MoO_3$ films grown on $SrTiO_3$(100) substrate (red, top), $SrTiO_3$ (110) substrate (blue, middle) and $SrTiO_3$(510) substrate (black, bottom), respectively. In all cases, four peaks at 10.93°, 21.94°, 28.27° and 39.03°, corresponding respectively to the $(20\bar{1})$, $(40\bar{2})$, (401) and (601) $K_{0.3}MoO_3$ crystal planes, are identifiable. For films grown on $SrTiO_3$(100) and $SrTiO_3$(110) substrates, an extra intense peak is visible in the respective XRD patterns. These originate from diffraction from the substrates themselves. The (100) diffraction peak is at 22.85° and the (110) at 32.46°.

In the case of growth on $SrTiO_3$(510) substrate (black, bottom), the diffraction pattern is dominated by a strong peak at 10.93° corresponding to the $(20\bar{1})$ plane, with the other 3 peaks displaying low intensity. It is noteworthy that the peak at 39.03° corresponding to the (601) plane, is comparable in

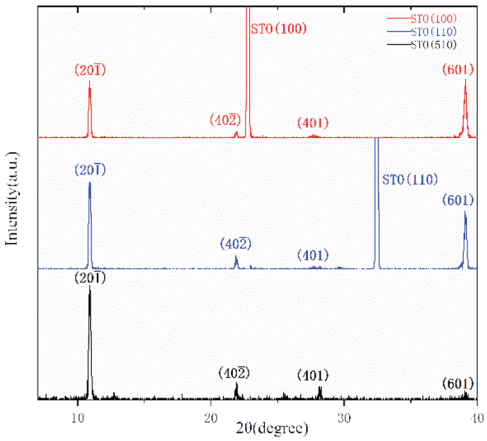

Fig. 1 XRD pattern of a $K_{0.3}MoO_3$ thin film grown on a $SrTiO_3$(100) substrate (red, top), $SrTiO_3$(110) substrate (blue, middle) and $SrTiO_3$(510) substrate (black, bottom). The peaks with extremely high intensity at 22.85°(red) and 32.46°(blue) corresponding to the substrate peaks of $SrTiO_3$(100) and $SrTiO_3$(110), respectively. The quasi-one dimensional (1D) chains lie in the $(20\bar{1})$ plane of $K_{0.3}MoO_3$, corresponding to the dominant peak at 10.93° on $SrTiO_3$(510) substrate(black). In the case of deposit on $SrTiO_3$(510), the (601) peak is rarely identifiable.

intensity to the $(20\bar{1})$ peak for the films grown on the $SrTiO_3$(100) substrate (red, top) and the $SrTiO_3$ (110) substrate (blue, middle), but is very weak for the films grown on $SrTiO_3$(510) substrate (black, bottom). The other two identifiable peaks at 21.94° and 28.27°, corresponding to the $(40\bar{2})$ and (401) planes, remain weak for growth on three substrates. We conclude that growth of the $K_{0.3}MoO_3$ films proceeds with the $(20\bar{1})$ plane parallel to the substrate, and that the film grown on the $SrTiO_3$(510) substrate is highly oriented. This conclusion is also supported by morphology characterization below.

Representative SEM images of $K_{0.3}MoO_3$ rod-shaped grains are shown in Fig. 2. The grains on different $SrTiO_3$ substrates are all of the order of micrometers in size and show heteroepitaxial growth along different preferential orientations depending on the substrates. Fig. 2(a) shows a $K_{0.3}MoO_3$ thin film grown on $SrTiO_3$(100). The rod-shaped grains run parallel to both the $SrTiO_3$(100) [010] and [001] axes and this is explained by the crystal structure of the substrate. $SrTiO_3$ is a cubic perovskite crystal with lattice parameters $a = b = c =$ 3.905 Å,[15] while the width of the quasi-1D $K_{0.3}MoO_3$ chains is $b = 7.552$ Å. The mismatch of between $2a = 7.810$ Å for $SrTiO_3$ and the width of $K_{0.3}MoO_3$ chains is as small as 3.3% and the square symmetry of the $SrTiO_3$(100) surface allows the $K_{0.3}MoO_3$ chains to grow in two perpendicular directions.

In contrast, the $K_{0.3}MoO_3$ thin films exhibit only one preferential growth direction on the $SrTiO_3$(510) substrate as shown in Fig. 2(b). The $K_{0.3}MoO_3$ $(20\bar{1})$ plane is parallel to the $SrTiO_3$(510) plane and the interfacial match is shown in Fig. 3 with a 3.3% mismatch in one direction (the same as for the $SrTiO_3$(100) substrate) and a 0.7% mismatch in the $[\bar{1}50]$ direction. The majority of the rod-shaped grains are along $[\bar{1}50]$ direction with few short grains along [001] direction.

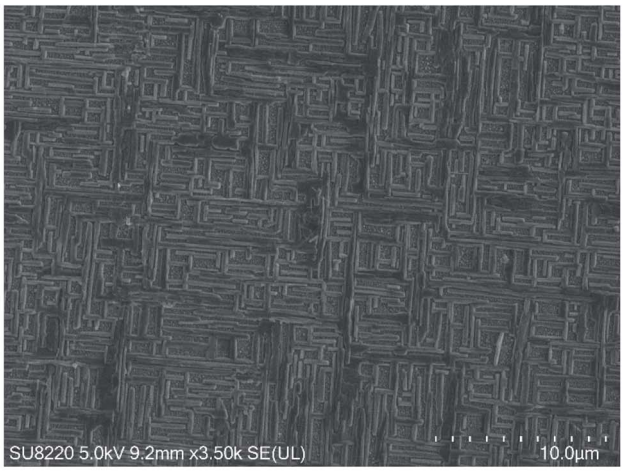

(a)

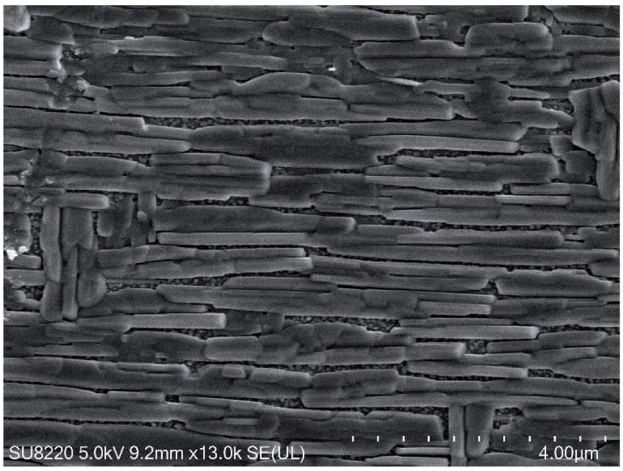

(b)

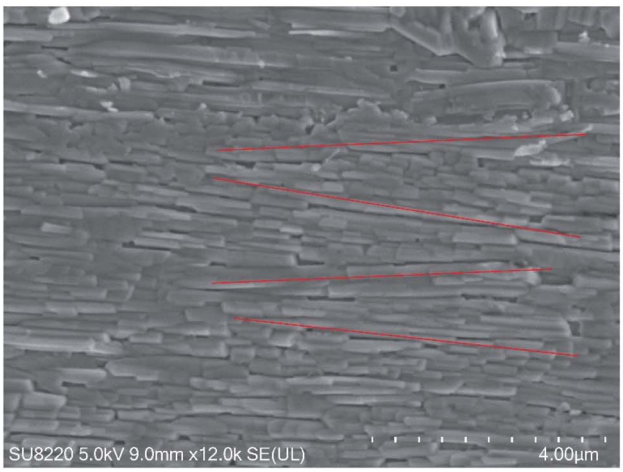

(c)

Fig. 2 Typical SEM images of $K_{0.3}MoO_3$ thin films grown (a) on $SrTiO_3(100)$, (b) on $SrTiO_3(510)$, (c) on $SrTiO_3(110)$, respectively. The red line on $SrTiO_3(110)$ suggest the multidirectional growth of grains comparing with the unidirectional growth of grains on $SrTiO_3(510)$.

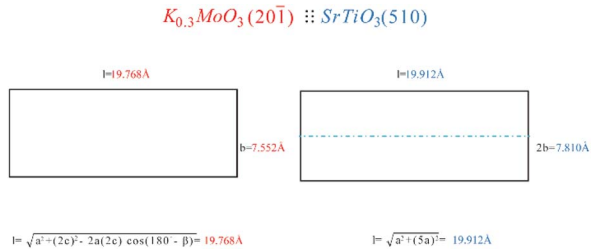

Fig. 3 Schematic of the lattice match leading to $K_{0.3}MoO_3$ (20$\bar{1}$) and $SrTiO_3$(510). The length of the $K_{0.3}MoO_3$ (20$\bar{1}$) lattice plane is calculated by cosine rule and the length of $SrTiO_3$(510) is calculated by Pythagorean theorem.

For growth of $K_{0.3}MoO_3$ on a $SrTiO_3$(110) substrate there is a 3.3% mismatch in the [001] direction and 11.7% mismatch in the [$\bar{1}$10] direction; the resulting SEM image from such a film is shown in Fig. 2(c). The $SrTiO_3$(110) plane does not have a square symmetry and does not match the $K_{0.3}MoO_3$ (20$\bar{1}$) plane as well as does the $SrTiO_3$(510) plane. The SEM image for $K_{0.3}MoO_3$ grown on $SrTiO_3$(110) is different from those from growth on $SrTiO_3$ (100) and $SrTiO_3$(510): the rod-shaped grains occur are found lying along several non-parallel directions (the red lines in Fig. 2(c) indicate the directions of the grains). We conclude that the most satisfactory epitaxial growth of $K_{0.3}MoO_3$ thin films occurs on a $SrTiO_3$(510) substrate.

The topology of the $K_{0.3}MoO_3$ thin films was measured using AFM as presented in Fig. 4. The AFM images not only show similar grain structure as the SEM images in Fig. 2, but we can also determine the thickness of the grains from these images. We find that the thickness of the films on both $SrTiO_3$(100) and $SrTiO_3$(510) substrates is approximately 100 nm.

3.2 Transport measurement

CDW phenomena tend to occur in chain compounds or layered structural materials where the CDW driven lattice distortion causes the metal to semiconductor transition. $K_{0.3}MoO_3$ has a chain structure with highly anisotropic charge transport: for single crystals, the resistivity (ρ) anisotropy ratio[16] is about 1 : 30 : 1000 with most conducting direction[17] $\rho \sim 5 \times 10^{-6}$ to 5 $\times$ 10^{-5} Ω m. The experimental configuration for our 4-point probe measurement of the anisotropic resistivity as well as the metal to semiconductor transition in our films is shown in Fig. 5. First the resistivity was measured along one axis of the $SrTiO_3$ substrate from 350 K to 90 K and then we rotated our substrate by 90° and measured along the other axis of the $SrTiO_3$ substrate again from 350 K to 90 K.

The temperature dependence of the electrical resistivity of the $K_{0.3}MoO_3$ thin films is shown in Fig. 6. For $SrTiO_3$(100) (Fig. 6(a)), the resistance does not show obvious variation along the [010] and [001] axes and this is anticipated from the square symmetry of the substrate. The resistivity can be calculated from $\rho = \frac{RA}{\ell}$ where R is the resistance, A is the cross-sectional area of the specimen, ℓ is the length of the sample. The resistance was $R(T = 0\ ^\circ\mathrm{C}) = 340\ \Omega$, the cross-sectional area is

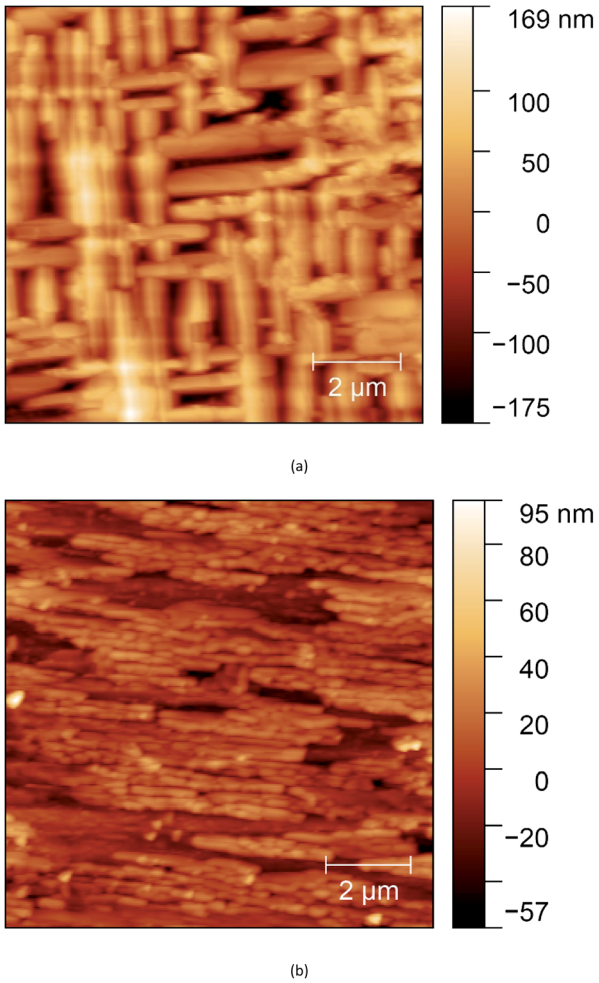

Fig. 4 Typical AFM images of $K_{0.3}MoO_3$ thin films grown (a) on $SrTiO_3$(100), (b) on $SrTiO_3$(510).

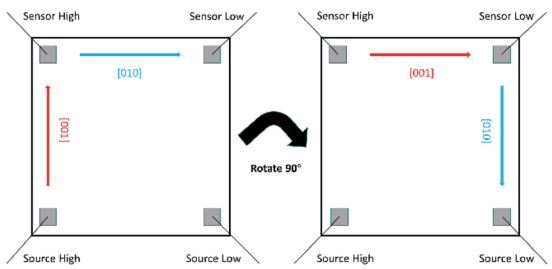

Fig. 5 Schematic of measuring the temperature dependence of resistivity of $K_{0.3}MoO_3$ on different $SrTiO_3$(100) axes by four-probe method. The gray squares represent the indium pads.

calculated by $A = ad$ where $a = 5$ mm is the length of the substrate and $d \sim 100$ nm is the thickness of the film, $\ell = a = 5$ mm is also the length of the square substrate. The calculated $\rho = 3.4 \times 10^{-5}$ Ω m is consistent with the resistivity of the most conducting direction of single crystal $K_{0.3}MoO_3$. It is also observed that below about 180 K, the resistance increases much more rapidly than above 180 K. This result is consistent

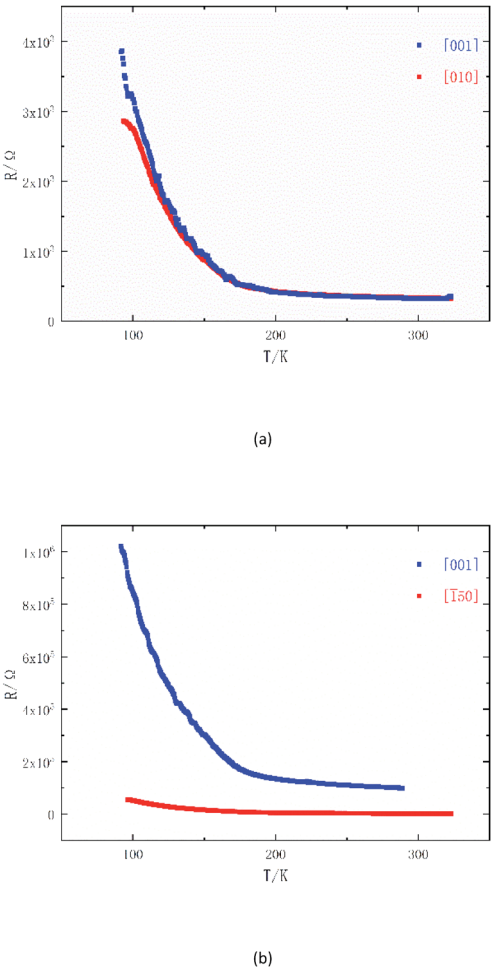

Fig. 6 The temperature dependence of resistance for $K_{0.3}MoO_3$ thin films grown (a) on $SrTiO_3$(100), (b) on $SrTiO_3$(510). The blue and red curve represent different lattice axes.

with the opening of a gap at E_F due to the Peierls transition, as in single crystal $K_{0.3}MoO_3$.

Fig. 6(b) shows the temperature dependence of the resistivity for blue bronze measuring along [001] and [1̄50] axes of $SrTiO_3$(510). Along [1̄50], $R(T = 0\ ^\circ C) \sim 2680$ Ω, while along [001] $R(T = 0\ ^\circ C) \sim 1 \times 10^5$ Ω. The resistance ratio is about 1 : 37, similar to the anisotropy ratio in single crystals. From the resistance ratio in Fig. 6(b), we conclude that the second most conducting direction for blue bronze is also parallel to the substrate. The temperature dependence of the resistance for films grown on $SrTiO_3$(510) is similar to those grown on $SrTiO_3$(100) where the metal to semiconductor transition occurred around 180 K. The resistance $R(T = 0\ ^\circ C)$ for films grown on $SrTiO_3$(510) along [1̄50] is larger than the $R(T = 0\ ^\circ C)$ for those grown on $SrTiO_3$(100); this may be due to variations in contact resistance, flatness of the film, or some unknown impurity.

4 Conclusions

We succeed in preparing high-quality crystalline $K_{0.3}MoO_3$ thin films by pulsed laser deposition on $SrTiO_3$(100), $SrTiO_3$(510)

and $SrTiO_3$(110) with thickness about 100 nm. The films were characterized by single crystal XRD, SEM, EDS, and AFM. Sample stoichiometry can be well controlled, and the morphology of the resulting films consists of $K_{0.3}MoO_3$ rods of variable sizes and depends on the substrate choice. The rods exhibit a square symmetry pattern on $SrTiO_3$(100), a unidirectional pattern on $SrTiO_3$(510), while on $SrTiO_3$(110) the rods align along various directions. The temperature dependence of the electrical resistance reveals a very large anisotropy, and also a metal to semiconductor transition at about 180 K. Our preliminary results demonstrated the possibility of growing crystalline $K_{0.3}MoO_3$ thin films with controllable size and quality when the growth conditions are further carefully optimized. This may facilitate novel investigations of collective phenomena such as Peierls transition, periodic lattice distortions and CDWs in quasi-low dimensional solids.

Conflicts of interest

There are no conflicts to declare.

Acknowledgements

The authors acknowledge support from the Institute of Physics, Chinese Academy of Sciences for the PLD equipment.

Notes and references

1 C. Schlenker, J. Dumas, C. Escribe-Filippini and H. Guyot, in *Low-Dimensional Electronic Properties of Molybdenum Bronzes and Oxides*, Springer, 1989, pp. 159–257.
2 C. Schlenker, J. Dumas, C. Escribe-Filippini, H. Guyot, J. Marcus and G. Fourcaudot, *Philos. Mag. B*, 1985, **52**, 643–667.
3 M. Keizo, W. Yufeng, S. Yuki, T. Natarajan Rani, K. Kensuke, A. Sonachalam, T. Yusaku, Y. Harukazu and K. Reizo, *Synth. Met.*, 2009, **159**, 2397–2398.
4 M. Greenblatt, *Chem. Rev.*, 1988, **88**, 31–53.
5 G. H. Bouchard Jr, J. H. Perlstein and M. J. Sienko, *Inorg. Chem.*, 1967, **6**, 1682–1685.
6 J. Graham and A. Wadsley, *Acta Crystallogr.*, 1966, **20**, 93–100.
7 P. Monceau, N. Ong, A. M. Portis, A. Meerschaut and J. Rouxel, *Phys. Rev. Lett.*, 1976, **37**, 602.
8 M. Itkis, F. Y. Nad and P. Monceau, *J. Phys.: Condens. Matter*, 1990, **2**, 8327.
9 A. Wold, W. Kunnmann, R. Arnott and A. Ferretti, *Inorg. Chem.*, 1964, **3**, 545–547.
10 R. Thorne, *Phys. Rev. B: Condens. Matter Mater. Phys.*, 1992, **45**, 5804.
11 D. Borodin, S. Zaitsev-Zotov and F. Y. Nad, *Zh. Eksp. Teor. Fiz.*, 1987, **93**, 1394–1409.
12 T. Nishida and K. Eda, *J. Nanopart. Res.*, 2018, **20**, 27.
13 H. Van Der Zant, O. Mantel, C. Dekker, J. Mooij and C. Træholt, *Appl. Phys. Lett.*, 1996, **68**, 3823–3825.
14 D. Dominko, D. Starešinić, K. Salamon, K. Biljaković, A. Tomeljak, H. Schäfer, T. Huber, J. Demsar, G. Socol and C. Ristoscu, *J. Appl. Phys.*, 2011, **110**, 014907.
15 M. Schmidbauer, A. Kwasniewski and J. Schwarzkopf, *Acta Crystallogr., Sect. B: Struct. Sci.*, 2012, **68**, 8–14.
16 J. Pouget, S. Kagoshima, C. Schlenker and J. Marcus, *J. Phys., Lett.*, 1983, **44**, 113–120.
17 W. Fogle and J. H. Perlstein, *Phys. Rev. B: Solid State*, 1972, **6**, 1402.